Sanchis-Perucho, P.; Robles, Á.; Durán, F.; Rogalla, F.; Ferrer, J.; Seco, A. (2021). Widening the applicability of AnMBR for urban wastewater treatment through PDMS membranes for dissolved methane capture: Effect of temperature and hydrodynamics. Journal of Environmental Management. 287:1-11. https://doi.org/10.1016/j.jenvman.2021.112344

Widening the applicability of AnMBR for urban wastewater treatment through PDMS membranes for dissolved methane capture: Effect of temperature and hydrodynamics.

Pau Sanchis-Perucho [a*], Ángel Robles [a], Freddy Durán [b], Frank Rogalla [b], José Ferrer [c], Aurora Seco [a]

[a] CALAGUA – Unidad Mixta UV-UPV, Departament d'Enginyeria Química, Universitat de València, Spain. (e-mail: pau.sanchis-perucho@uv.es; angel.robles@uv.es; aurora.seco@uv.es)

[b] FCC Aqualia, S.A., Spain. (e-mail: freddy.duran@fcc.es; FRogalla@fcc.es)

[c] CALAGUA – Unidad Mixta UV-UPV, Institut Universitari d'Investigació d'Enginyeria de l'Aigua i Medi Ambient – IIAMA, Universitat Politècnica de Valencia, Spain. (e-mail: jferrer@hma.upv.es)

*Corresponding author

ABSTRACT

AnMBR technology is a promising alternative to achieve future energy-efficiency and environmental-friendly urban wastewater (UWW) treatment. However, the large amount of dissolved methane lost in the effluent represents a potential high environmental impact that hinder the feasibility of this technology for full-scale applications. The use of degassing membranes (DM) to capture the dissolved methane from AnMBR effluents can be considered as an interesting alternative to solve this problem although further research is required to assess the suitability of this emerging technology. The aim of this study was to assess the effect of operating temperature and hydrodynamics on the capture of dissolved methane from AnMBR effluents by DMs. To this aim, a commercial polydimethylsiloxane (PDMS) DM was coupled to an industrial prototype AnMBR (demonstration scale) treating UWW at ambient temperature. Different operating temperatures have been evaluated: 11, 18, 24 and 30 ºC. Moreover, the DM was operated at different ratios of liquid flow rate to membrane area (Q_L:A) ranging from 22 to 190 $Lh^{-1}m^{-2}$ in order to study the resistance of the system to methane permeation. Methane recovery was maximized when temperature raised and Q_L:A was reduced, giving methane recovery efficiencies (MRE) of about 85% at a temperature of 30 ºC and a Q_L:A of 25 $Lh^{-1}m^{-2}$. The study showed that high Q_L:A ratios hinder methane recovery by the perturbation of the DM fibers, being this effect intensified at lower temperatures probably due the higher liquid viscosities. Also, the performed fouling evaluation showed that not significant membrane fouling may be expected in the DM unit at the short-term when treating AnMBR effluents. A resistance-in-series model was proposed to predict the overall mass transfer of the system according to operating temperature and Q_L:A, showing that methane capture was controlled by the liquid phase, which represented up to 80-90% of total mass transfer resistance. The energy and environmental evaluation performed in

this study revealed that PDMS DMs would enhance energy recovery and environmental feasibility of AnMBR technology for UWW treatment, especially when operating at low temperatures. When MRE was maximized, the combination of AnMBR with DM achieved net energy productions and net greenhouse gas reductions of up to 0.87 kWh and 0.216 kg CO_2–eq per m^3 of treated water.

Keywords

Anaerobic membrane bioreactor (AnMBR); greenhouse gas (GHG) emissions; dissolved methane capture; PDMS degassing membrane; urban wastewater.

1. INTRODUCTION

Water stress is now a serious and growing problem worldwide and there is an urgent need to apply a new wastewater development model focused on the Circular Economy. In view of the current global energy crisis and climate change, a more energy-efficient and environmentally-friendly technology is required able to generate high-quality reclaimed water. In the wastewater sector, aerobic-based treatments are identified as energy-intensive processes due to the large amount of energy required to oxidize organic waste (Lee *et al*., 2017), while high biosolid production rates can also be expected in aerobic systems (McCarty *et al*., 2011). On the other hand, anaerobic processes avoid aeration requirements when transforming biodegradable material into methane. However, due to the lower growth rate of anaerobic microbes, high-rate processes are needed for treating urbane wastewaters (UWW) anaerobically to reduce capital costs (i.e. reducing reactor volume).

Anaerobic membrane bioreactors (AnMBRs) have been proposed by several authors as a suitable alternative for high-rate UWW treatment. Thanks to membrane technology, sludge and hydraulic retention times can be decoupled allowing the retention of generated biomass (Giménez *et al.*, 2012; Smith *et al*., 2012) while producing a high quality effluent (solids-free). Nevertheless, AnMBR systems still present different key issues that restrict their implementation in full-scale UWW treatments (Robles *et al.*, 2018), being one of the main drawbacks the direct greenhouse gas (GHG) emissions produced by stripping dissolved methane from the effluent which raise the carbon footprint and reduce process energy-efficiency (Smith *et al.*, 2012). Indeed, methane losses can reach up to 80% of the total methane production at relatively low operating temperatures (e.g. 15 ºC) (Giménez, *et al.*, 2014; Cookney *et al.*, 2016), so that efficient capture of the dissolved methane plays a crucial role in advancing AnMBR technology for UWW treatment.

Degassing membranes (DM) are a promising solution for capturing dissolved methane from anaerobic effluents (Crone *et al.*, 2017). This technology avoids the frequent degassing tower operating problems (e.g. flooding, foaming and emulsion) thanks to liquid and gas phase division by membranes (Stanojević *et al.*, 2003). The possibility of operating DMs in the vacuum mode also prevents captured methane dilution (characteristic of sweep gas processes), enhancing the potential energy valorization of recovered methane. In fact, recent studies have showed promising efficiencies for methane recovery from anaerobic effluents on a lab-scale (Bandara *et al.*, 2013; Cookney *et al.*, 2016; Henares *et al.*, 2017), proving the effectivity of DMs for this purpose. Nonetheless, further aspects need to be considered in order to evaluate the feasibility of this technology to support AnMBR technology, finding optimal conditions under which the energy recovery potential of the system is maximized and the GHG emissions are minimized.

One of most important issues to take into account is the operating temperature of the system. In anaerobic treatment, anaerobic reactor heating generally represents the major process energy input (Lettinga *et al.*, 2001; Bani *et al.*, 2009), suggesting ambient operation to reduce operating costs (Bandara *et al.*, 2011) and indirect GHG emissions (Bani *et al.*, 2009) when treating low-strength UWWs. In this context, AnMBR can be considered as an attractive option since the membrane allows operating at low/mild temperatures without compromising the effluent quality or process energy balance, reporting even net energy outputs in some cases (Pretel *et al.*, 2015; Stazi and Tomei, 2018). Nonetheless, since methane solubility in water increases as the operating temperature decreases, more methane losses are expected under these conditions (Velasco *et al.*, 2018). Therefore, evaluating methane capture efficiency of DMs at different temperatures is imperative to determine the most suitable operating conditions of the

combination AnMBR+DM, considering both environmental and energy aspects. On the other hand, since non-porous membranes provide a significant additional resistance for the methane capture, it is necessary to determine the main methane permeation resistance, as well as the conditions under which it is minimized, in order to maximize dissolved methane capture. In this regard, when using different DMs for dissolved gases recovery, Wickramasinghe *et al*. (1992) and Henares *et al.* (2017) showed that the liquid resistance is significatively superior than the membrane resistance or the gas resistance, revealing that the liquid flow rate plays a crucial role in methane permeation. Additionally, large-scale studies are needed to confirm the promising results reported for lab-scale membranes, considering the hydrodynamic changes of industrial DM modules compared to lab-scale DMs. Likewise, intrinsic variations when treating real UWWs such as the interactions among the different dissolved gases present in anaerobic effluents (e.g. carbon dioxide or sulfidic acid) or methane recovery reductions by membrane fouling need to be studied.

Therefore, this study aims to evaluate the effect of operating temperature and hydrodynamics on the performance of a commercial PDMS DMs for the capture of dissolved methane from the effluent of an industrial prototype AnMBR (demonstration-scale), which treated the effluent from the pre-treatment step of a full-scale WWTP. To this aim, the system was operated at 4 operating temperatures (11, 18, 24 and 30 ºC). Additionally, 8 liquid flow rates (from 22 to 190 $Lh^{-1}m^{-2}$) were tested in order to evaluate the resistance of the DM system to methane permeation at different conditions. Based on the experimental results, the better strategies that maximized methane recovery were determined. On the other hand, a resistance-in-series model was proposed to predict the DM's system methane capture resistance. Finally, the energy and environmental (GHG emissions) feasibility of the combined system (AnMBR+DM) was assessed.

2. MATERIALS AND METHODS

2.1. Experimental set-up

A polydimethylsiloxane (PDMS) hollow-fiber commercial module (PermSelect®, MedArray Inc. USA) was employed as DM for the treatment of the methane-saturated effluent from an AnMBR prototype-plant. The AnMBR prototype-plant consisted of a 40 m^3 anaerobic bioreactor coupled to three external membrane tanks (0.8 m^3 each). The membrane tanks were fitted with an ultrafiltration membrane system (PURON® PSH 41, Koch Membrane Systems, 0.03 μm pore size) giving 123 m^2 of total filtration area. This AnMBR system was installed in the 'Alcázar de San Juan' WWTP (Ciudad Real, Spain) and was fed with effluent from the pre-treatment step of the full-scale WWTP. Further information on this AnMBR system can be found in Jiménez *et al*. (2020). The average AnMBR effluent characteristics and operating conditions during the experimental periods can be found in the Appendix A, Table A1.

The DM unit was operated in shell-side mode to avoid lumen clogging-related problems (Sanchis-Perucho *et al*., 2020) with vacuum applied to the lumen side to provide the driving force. Previous studies have shown the favorable effects of operating PDMS DMs at high transmembrane pressures (TMP) (Cookney *et al.*, 2012; Henares *et al.*, 2017). In fact, the previous results obtained by the system (see Sanchis-Perucho *et al*., 2020) revealed that net energy recovery can be maximized by increasing TMP. Since the DM unit had a limit shell-side operating pressure of 1 bar, TMP was set to 0.8 bar to avoid operating close to the permitted maximum. Two pressure sensors (UNIK 5000-746-3600, Druck) were fitted to the liquid and gas sides for continuous TMP monitoring and control. The main features of the DM module can be found in the Appendix B, Table B1.

The AnMBR+DM combination was operated at ambient temperatures of 11, 18, 24 and 30 ºC to assess the effect of seasonal temperature dynamics on methane capture efficiency and AnMBR+DM system energy and environmental feasibility. The liquid flow rate to membrane area (Q_L:A) ratio was varied from 22 to 190 $Lh^{-1}m^{-2}$ with a stepwise of 24 $Lh^{-1}m^{-2}$. A liquid-flow meter (VX100-45, Vogelsang) was used to measure the applied Q_L:A.

2.2. Analytical methods

Duplicate liquid samples from the DM inlet and outlet were collected in 50 mL glass vials and stored at 20 ºC with continuous stirring for at least 4 hours to reach gas-liquid thermodynamic equilibrium. The DM unit was operated for at least 5 minutes before the sampling to achieve steady-state conditions. Methane concentration in the head-space of the vials was determined by gas chromatography. Further details on the method used to determine dissolved methane concentrations and calculate the amount of methane recovered can be found in Sanchis-Perucho *et al*. (2020).

To evaluate potential fouling issues during DM operation, the concentrations of ammonium, phosphate, total organic carbon (TOC), and total inorganic carbon (TIC) were determined in the DM inlet and outlet streams at different Q_L:A ratios. Ammonium and phosphate concentrations were obtained according to Standard Methods (APHA AWWA WEF, 2012). TOC and total carbon (TC) concentrations were determined by a TOC-VCHS total organic carbon analyzer (Shimazu Corporation), determining the TIC concentration by difference.

2.3. Calculations

2.3.1. Evaluation of DM performance

Methane recovery efficiency (MRE), net energy demand, and GHG emissions in the DM unit were calculated according to the method described in Sanchis-Perucho *et al*. (2020). The AnMBR energy demand was theoretically calculated according to Pretel *et al.* (2016) using data from the AnMBR prototype-plant: equipment, flows, biogas production, operating temperature, etc. AnMBR GHG emissions were calculated considering both energy savings and dissolved methane lost into the effluent.

Liquid velocity (v_L) and Reynolds module (Re) were determined for DM hydrodynamics evaluation. Since the membrane was operated on the shell side, which had an enhanced hydrodynamic structure to improve dissolved gas recovery, v_L and Re were calculated accounting for an equivalent diameter (D_{eq}). A diagram of the commercial DM unit used in this study can be found in the Appendix B, Fig. B1. The DM unit had a central cylindrical diffuser to improve the contact between the liquid and the membrane while reducing the dead zones, so that two different liquid fluxes could be considered in the system: (1) a flux parallel to the fibers across the annular DM section, and (2) a flux perpendicular to the fibers from the cylindrical diffuser to the DM external diameter. Although the fluxes were simultaneous and affected DM hydrodynamics, in order to simplify the calculation both v_L and Re were calculated assuming that the liquid flux was controlled by a single mechanism. According to this simplification, similar v_L and Re values were obtained regardless of the flux considered (data not shown). Since the perpendicular flux requires more factors to be considered (e.g. fiber distribution, number of fibers in each section pass, average distance between fibers, etc.), D_{eq} was estimated with the parallel flux as the dominant mechanism using the following expression:

$$D_{eq} = \sqrt{\frac{4 \cdot (V_S - V_{cd})}{\pi \cdot L_w}} \quad eq.(1)$$

Where V_S and V_{cd} are the DM unit shell volume and the cylindrical diffuser volume, respectively, and L_w is the wet fiber length (see Table 1 and Fig. 1).

2.3.2. Theory approach on DMs overall mass transfer coefficient

Dissolved gas capture by DMs can be modeled considering the different involved phases as an ideal three resistance-in-series system. Defining the total mass flux resistance (R_T) as the inverse of the overall mass transfer coefficient (K_O), the R_T can then be obtained from the total of the different resistances involved in the methane mass capture: the liquid boundary layer (R_L), the permeable non-porous membrane (R_M) and the gas phase boundary layer (R_G). Considering cylindrical coordinates, the resistance-in-series model can be expressed as follows:

$$R_T = \frac{1}{K_O\, A_L} = \frac{1}{k_L A_L} + \frac{1}{k_M\, A_{ml}} + \frac{1}{H^{CH4}(T)\, k_G\, A_G} = R_L + R_M + R_G \quad eq.(2)$$

Where k_L, k_M and k_G are the gas mass transfer coefficients in liquid, membrane and gas phases, respectively, A_L and A_G are the effective membrane area interacting with liquid and gas phases, respectively, A_{ml} is the logarithmic mean area of the DM and $H^{CH4}(T)$ is the Henrry's constant for methane. However, unlike the liquid and membrane phases, the gas boundary layer does not usually represent a significant resistance to mass flux due to the higher diffusion coefficients in gases than in liquids and membranes (Lu *et al.*, 2008). *Eq.* (2) is therefore commonly simplified into the following expression:

$$\frac{1}{K_O\, A_L} = \frac{1}{k_L\, A_L} + \frac{1}{k_m\, A_{lm}} \quad eq.(3)$$

Considering the different described resistances as an isotropic material, the one-dimensional Fick's first law (steady state) can be used to calculate the gas flux through the membrane in dissolved gas capture systems:

$$J = -D\frac{dc}{dx} \quad eq.(4)$$

Where J represents the flux, c the concentration of the diffused compound, x the distance and D the diffusion coefficient. Applying *eq.* (4) on the liquid phase, the following expression can then be obtained:

$$J = \frac{D_{CH4-W}}{t_L} \cdot \Delta c = k_L \cdot \Delta c \quad eq.(5)$$

Where $D_{CH4\text{-}W}$ is the methane diffusion coefficient in water and t_L is the thickness of the liquid phase resistance. Since methane is homogeneously dissolved in the DM's influent, t_L can be considered as the liquid phase boundary thickness, which should depend on operating v_L. $D_{CH4\text{-}W}$ can be influenced by both v_L and temperature. The temperature effect on $D_{CH4\text{-}W}$ can be represented by the equation proposed by Himmelblau (1964):

$$D_{CH4-W} = exp\left(\frac{-A}{T} + B\right) \cdot 10^{-9} \quad eq.(6)$$

Where T is the temperature and A and B are fitting parameters that depend on the diffusing specie and the medium (Himmelblau, 1964). Alternatively, considering turbulent liquid conditions in cylindrical pipes, the Linton & Sherwood semi-empirical expression can be used to estimate k_L:

$$\frac{k_L \cdot D_{eq}}{D_{CH4-W}} = Sh = 0.023 \cdot Re^{0.83} \cdot Sc^{1/3} \quad eq.(7)$$

Where Sh and Sc are the Sherwood and Schmidt dimensionless modules, respectively.

On the other hand, a similar expression to *eq.* (5) can be obtained when applying Fick's law to the membrane phase. In non-porous membranes, membrane resistance is usually modeled by the solubility-diffusion theory (Tremblay *et al.*, 2006), according to which mass transport through dense membranes is carried out in three steps: (1) gas is dissolved on the membrane surface, (2) diffused across the membrane, and (3) re-dissolved in the gas phase. Defining membrane permeability as solubility and diffusivity product (*i.e.* P=S·D) (Tremblay *et al.*, 2006), Fick's first law applied to non-porous membrane systems can thus be expressed as follows:

$$J = \frac{P_{CH4-PDMS}}{t_M} \cdot \Delta c = \frac{S_{CH4-PDMS} \cdot D_{CH4-PDMS}}{t_M} \cdot \Delta c = k_M \cdot \Delta c \quad eq.(8)$$

Where t_M is membrane thickness and $D_{CH4\text{-}PDMS}$, $S_{CH4\text{-}PDMS}$ and $P_{CH4\text{-}PDMS}$ are methane diffusion, solubility and permeability in PDMS material, respectively. In this case, the influence of temperature on non-porous membrane permeability can be calculated by the Van't Hoff–Arrhenius approach (Raharjo *et al.*, 2007a):

$$P_{CH4-PDMS} = P_0 \cdot exp\left(\frac{-E_P}{R \cdot T}\right) \quad eq.(9)$$

Where R is the universal constant of gases (0.082 atm L mol^{-1} K^{-1}), P_0 is the pre-exponential factor and E_P is the activation energy of permeation. Finally, *eqs*. (5) and (8) can be combined and included in *eq.* (3), resulting in the following expression which can be used to predict K_O regarding temperature.

$$K_O = \left(\frac{1}{\frac{t_L}{exp\left(\frac{-A}{T}+B\right)\cdot 10^{-9}\cdot A_L} + \frac{t_M}{P_0 \cdot exp\left(\frac{-E_P}{RT}\right)\cdot A_{lm}}}\right)\frac{1}{A_L} \quad eq.(10)$$

Alternatively, using the turbulent model to estimate k_L, a similar expression can be obtained:

$$K_O = \left(\frac{1}{\frac{D_{eq}}{0.023 \cdot Re^{0.83} \cdot Sc^{1/3} \cdot D_{CH4-W} \cdot A_L} + \frac{t_M}{P_0 \cdot exp\left(\frac{-E_P}{RT}\right) \cdot A_{lm}}} \right) \frac{1}{A_L} \quad eq.(11)$$

2.3.3. Experimental determination of DMs overall mass transfer coefficient

K_O in DMs can be calculated applying a dissolved methane mass balance in the liquid phase (Wickramasinghe *et al.*, 1993):

$$Q_L \, dc_{CH4} = J_{CH4} \, dA_M \quad eq.(12)$$

Where Q_L is the liquid flow rate pumped through the DM unit, A_M is the membrane area, c_{CH4} is the dissolved methane concentration in the water and J_{CH4} is the permeated methane flux, which is perpendicular to the liquid flux. Then, applying Fick's first law in *eq.* (12) and rearranging the expression, the following differential equation is obtained (Wickramasinghe *et al.*, 1993):

$$Q_L \frac{dc_{CH4}}{dA_M} + K_O(c_{CH4} - c^*_{CH4}) = 0 \quad eq.(13)$$

Where c^*_{CH4} is the membrane-gas interphase methane concentration, which is normally estimated considering equilibrium conditions between c^*_{CH4} and the methane concentration reached in the gas phase (C_G) (Cookney *et al.*, 2016; Henares *et al.*, 2017):

$$c^*_{CH4} = H^{CH4}(T) \cdot c_G \quad eq.(14)$$

Assuming an average constant value for c_G at each operating temperature, *eq.* (13) can be integrated between the influent and effluent methane concentration in the DM, resulting in the following equation:

$$K_O = -\frac{Q_L}{A_M} \ln\left(\frac{c_{CH4.eff} - c^*_{CH4}}{c_{CH4.inf} - c^*_{CH4}}\right) \quad eq.(15)$$

285 Where $c_{CH4.inf}$ and $c_{CH4.eff}$ are the concentrations of dissolved methane in influent and
286 effluent membrane streams, respectively. Since continuous vacuum was employed to
287 provide the driving force for the methane capture and k_G was assumed as negligible, the
288 c^*_{CH4} reached during DM operations was considered negligible compared to the c_{CH4}
289 present in the liquid phase (*i.e.* $c_{CH4} >>> c^*_{CH4}$, thus $c_{CH4} - c^*_{CH4} \approx c_{CH4}$). Therefore, *eq.*
290 (15) can be simplified to obtain *eq.* (16), resulting in an expression on which K_O can be
291 experimentally modeled for the operating conditions.

292 $$K_O = -\frac{Q_L}{A_M} \ln\left(\frac{c_{CH4.eff}}{c_{CH4.inf}}\right) \quad eq.(16)$$

293 The least squares method was used to adjust the theoretical K_O values calculated by *eqs.*
294 (10) and (11) to that obtained experimentally, estimating the value of the different
295 parameters (A, B, t_L, P_0 and E_P) for each Q_L:A ratio evaluated.

296 ## 3. RESULTS AND DISCUSSION

297 ### 3.1. Effect of operating conditions on methane recovery

298 Fig. 1 shows the recovered methane fluxes and methane recovery efficiencies reached by
299 the DM module under the evaluated operating conditions. As expected, temperature
300 played an important role in methane recovery. According to Fick's first law, methane flux
301 is controlled by both K_O and the methane concentration gradient. The higher the
302 temperature the lower the concentration of methane dissolved in the influent but the
303 higher K_O achieved (see Section 3.2). Due to this competitive effects, two different
304 dynamics can be observed regarding temperature rise. When low Q_L:A ratios were
305 applied, lightly lower methane fluxes where reached as temperature raised due the
306 reduction of the driving force (see Fig. 1a) but when the Q_L:A reached values around 100-

150 $Lh^{-1}m^{-2}$, K_O fell thus reducing the methane flux. Over these higher Q_L:A values, the higher methane fluxes achieved at higher temperatures (see Fig. 1b) were due to the early drop in K_O achieved at lower temperatures, hindering methane permeation. These dynamics also influenced MRE; it improved at high temperatures as shown in Fig. 1c. In this case, although in some circumstances higher methane fluxes can be achieved at lower temperatures, the higher K_O values and lower influent dissolved methane concentrations reached at higher temperatures increased the percentage of dissolved methane captured, showing that lower methane emissions can in fact be achieved at higher temperatures. This finding is in agreement with those reported by Cookney *et al*. (2011), who found improved methane recovery efficiencies in the summer period using PDMS membranes. Similarly, Bandara *et al*. (2012) reported slight higher dissolved methane emissions when operating a multi-layer polyethylene DM module in the winter period, although in this case lightly lower methane recovery efficiencies were achieved as temperature raised.

Regarding the effect of Q_L:A on MRE, the recovered methane flux increased progressively as Q_L:A was increased from 22 to 118 $Lh^{-1}m^{-2}$ (see Fig. 1a). However, a decrease in the recovered methane flux was observed at Q_L:A above 118 $Lh^{-1}m^{-2}$ (see Fig. 1b). As reported in other studies (Henares *et al*., 2017; Sanchis-Perucho *et al.*, 2020), this effect is related to a drop in K_O at high operating Q_L:A ratios (see Section 3.2), representing a negative effect on the methane flux through the membrane. On the other hand, as reported in a previous work (Sanchis-Perucho et al., 2020), raising Q_L:A negatively affected the MRE due the DM hydraulic retention time reduction (see Fig. 1c). Indeed, similar results were reported by Cookney *et al*. (2016) when operating a dense and micro-porous DM modules. Therefore, it can be concluded that when operating a PDMS DM module, lower dissolved methane emissions are expected at higher temperatures and lower Q_L:A ratios.

3.2. Influence of operating conditions on K_O

As exposed above, since K_O may control the amount of dissolved methane than can be captured form the treated liquid stream, maximizing K_O is necessary to boost DM effectivity. Then, K_O was calculated by *eq.* (16) for the different operating conditions evaluated to determine the most favorable conditions that maximized K_O. As can be seen in Fig. 2, raising the temperature had a favorable effect on K_O. As different in-series resistances are involved in DM methane recovery, temperature is expected to play a crucial role on K_O dynamics since methane solubility and diffusivity in water and PDMS are strongly affected by temperature. On the one hand, methane solubility in water is reduced at higher temperatures and the reduced driving force may decrease the amount of permeated methane, but should not directly affect k_L. In regard of methane diffusion in water, it is expected to increase at higher temperatures (Chen *et al*., 2018), enhancing k_L and therefore K_O. Thus, it could be assumed that the temperature rise reduced the liquid phase resistance to methane capture. On the other hand, considering gas solubility and diffusivity on PDMS membranes, a direct relationship between temperature and k_M cannot be deduced, since their effect on membrane permeability depends on the treated gas (Pinnau & He, 2004). Regarding methane solubility on PDMS, an increase in temperature reduces gas solubility on the membrane surface (Raharjo *et al.*, 2007b; Favre, 2017), thus reducing k_M. This effect is especially important for heavier gases, such as C_3H_8 (Sadrzadeh *et al.*, 2009), although methane solubility is slightly affected by temperature due to its lower molecular weight (Sadrzadeh *et al*., 2009). Hence, the negative effect of temperature on k_M may not strongly contribute to K_O. Conversely, a rise in temperature favors gas diffusion through the membrane. According to the free-volume theory (Stern, 1994), this phenomenon is due to an increase in polymeric chain structure mobility as temperature rises, allowing higher free volumes in the membrane structure and improving

gas diffusivity (Favre, 2017). Indeed, enhanced methane diffusion has been reported when raising the temperature in PDMS membranes (Raharjo et al., 2007a; Sadrzadeh *et al*., 2009) and improved methane permeability of PDMS membranes has been reported when increasing temperature in pure gas streams (Pinnau & He, 2004; Raharjo et al., 2007a; Sadrzadeh *et al*., 2009). Hence, it can be concluded that in dissolved methane capture by PDMS membranes a favorable effect on k_M can be achieved when operating at higher temperatures finally increasing K_O.

Concerning the effect of Q_L:A on K_O, increasing Q_L:A improved K_O to a maximum value, after which it fell as Q_L:A was raised (see Fig. 2a). As reported in a previous work (Sanchis-Perucho *et al*., 2020), this phenomenon could be explained by two possible hypotheses: either (1) the appearance of an additional mass transfer resistance or, (2) changes in the membrane hydrodynamic performance. A preliminary membrane fouling and hydrodynamic study was performed to determine the predominant reason why K_O falls at high Q_L:A ratios.

3.2.1. Short-term DM fouling evaluation.

As membrane fouling is one of most important issues in any membrane system, reduction of DM methane recovery capacity by reversible and/or irreversible fouling should be considered. In this respect, AnMBR effluent has a high-quality stream (solid-free permeate), thus reducing the possibility of a biological and/or inorganic cake layer forming on the DM membrane surface. Membrane fouling should therefore be controlled by the partial loss of the useful membrane area for depositing colloidal particles, salt precipitation or soluble compound adsorption on the membrane surface.

Table 1 shows the main characteristics of the DM influent and effluent streams. Since the higher the Q_L:A the higher the amount of described pollutants that can reach the

membrane surface, fouling propensity could be intensified as Q_L:A raises. However, no relevant changes were seen in the inlet and outlet nutrient concentrations and there were negligible changes in the TIC and TOC concentrations (without considering the captured methane). The results obtained thus seem to indicate that inorganic salt precipitation and/or organic substance adsorption did not contribute a great deal to short-term membrane fouling. Nevertheless, these substances could be deposited quite slowly, which makes their early identification difficult by regular sampling. Further studies are required to assess the possible unfavorable effects of these substances on DM performance and should focus on evaluating long-term fouling and consider integrated DM effluent sampling.

Three short-term fouling experiments were also performed. In this case, the DM module was operated for 90 minutes to evaluate the fouling rate under different Q_L:A ratios. Negligible MRE reductions were found during operations, indicating no fouling-related problems (see Fig. 3). This agrees with the results reported by Henares *et al.* (2017), who found not serious fouling problems until about 50 hours when operating a PDMS DM unit in shell-side mode. In addition, Bandara *et al*. (2012) not reported meaningful fouling propensities when operating a multi-layer polyethylene DM module for 18 months, concluding that membrane fouling is neither an important issue in the middle-term.

3.2.2. DM hydrodynamics evaluation

Liquid velocity and Reynolds number were calculated to study the hydrodynamic effects of raising Q_L:A. As can be seen in Fig. 2b, K_O declined at Reynolds numbers about 2100 - 4000, indicating a transition from laminar to turbulent flow. The K_O decline could thus be controlled in the studied operating conditions by the increasing turbulent flow. As Henares *et al*. (2017) have indicated, DMs can present a critical Q_L:A at which membrane

405 fibers may be less effective. This phenomenon can be explained by the greater shaking,
406 compression and deformation of membrane fibers as Q_L:A rises. The dead zones may also
407 increase when raising v_Ls on high fiber-density DMs (Coockney *et al*., 2011), especially
408 when operating on the shell side. Moreover, as Coockney *et al.* (2011) suggested, low
409 liquid velocities could help the development of a liquid-phase boundary layer that builds
410 up gas near the membrane surface and the greater turbulence would hinder methane
411 diffusivity through the membrane by reducing or removing this boundary layer.
412 Assuming that the reduced K_O was caused by the change in hydrodynamics, the earlier
413 drop of K_O at lower temperatures could have been caused by greater liquid viscosity. This
414 effect, although it can postpone turbulent flux development, would also result in a higher
415 liquid-fiber friction as Q_L:A grows, being able to increase fiber deformation and finally
416 decreasing more intensively the K_O at low temperatures. However, other undesirable
417 effects can also appear when raising Q_L:A, such as concentration polarization due the
418 increase in concentration gradients that oppose flux. Further research is required to
419 confirm this hypothesis.

420 ### 3.3. K_O-temperature modeling

421 The influence of temperature on K_O was first modeled by *eq.* (10). As can be seen in Fig.
422 4, the model accurately fitted the experimental data when operating at Q_L:A ratios lower
423 than 100 $Lh^{-1}m^{-2}$ but was slightly worse at higher Q_L:A ratios. This was mainly attributed
424 to the change in the DM flow conditions as v_L increased (see Fig. 2). In this respect, when
425 analyzing the values obtained for the different equation parameters (see Fig. 5),
426 parameters P_0 and E_P (methane-membrane permeability related parameters) remained
427 nearly invariable as Q_L:A was raised. This, as expected, confirms that k_M is not influenced
428 by the applied Q_L:A. However, a significant increase in parameters A and B (methane-
429 liquid diffusion related parameters) occurred at Q_L:A ratios over 100 $Lh^{-1}m^{-2}$. Indeed, the

values obtained for these parameters when operating at Q_L:A ratios under 100 $Lh^{-1}m^{-2}$ can be assumed as constant, achieving values of 1525±289 and 5.24±1.24 for A and B, respectively. These values are similar to those reported for convective methane diffusion in water (A=1990; B=7.11) (Chen *et al.*, 2018). The proposed model therefore agrees with previous conclusions indicating that for Q_L:A ratios over 100 $Lh^{-1}m^{-2}$ the flow inside the DM loses its laminar properties. Moreover, t_L fell slightly when the Q_L:A ratio was over 100 $Lh^{-1}m^{-2}$ (from 52.5±1.6 to 43.6±4.5 μm) which could represent the reduction in the liquid boundary layer due to increasing flow turbulence as v_L was raised. Nevertheless, although t_L fell by 20%, there was no clear correlation as v_L increased, so that no definite conclusions could be reached.

Since changes in the hydrodynamic conditions were not captured by the model proposed in *eq.* (10), an alternative turbulent model was used to represent K_O (*eq.* (11)). However, similar results were achieved in this case (see. Fig. 4), which could indicate that turbulent mass transfer diffusion dynamics were not the main controlling mechanism. Indeed, lower $D_{CH4\text{-}W}$ was reached than that expected in laminar conditions for Q_L:A values above 100 $Lh^{-1}m^{-2}$ (data not shown). This could indicate that the modeled k_L may be overestimated. As previously commented, disturbances on the fibers caused by the turbulent medium could reduce methane mass transfer. These effects may also be greater at low temperatures by a rise in medium viscosity. To estimate the disturbing effects of liquid flow on membrane fibers, the liquid viscosity was thus selected as the main variable to correct the modeled k_L values. This correction was applied considering a linear relationship between liquid viscosity and the disturbing effects on the membrane fibers, so that *eq.* (10) could be modified as follows:

$$K_O = \left(\frac{1}{\frac{t_L}{\left(exp\left(\frac{-A}{T}+B\right)\cdot 10^{-9}-(a+b\cdot\mu)\right)\cdot A_L} + \frac{t_M}{P_0\cdot exp\left(\frac{-E_P}{RT}\right)\cdot A_{lm}}} \right) \frac{1}{A_L} \quad eq.(17)$$

Where μ is the liquid dynamic viscosity, and a and b are linear fitting parameters. Since unfavorable effects on k_L should fall on the linear correction, in order to fit *eq.* (17) at high Q_L:A ratios, the liquid diffusion parameters (A and B) were fixed to the values determined in laminar conditions (i.e. 1525 and 5.24 for parameters A and B, respectively). The least squares method was also used to fit parameters a and b.

Eq. (17) properly fitted the experimental data (see Fig. 4), showing that viscosity could be used to correct the overestimated k_L values. Increasing linear values were achieved for the parameter a, representing the unfavorable effect of raising Q_L:A on K_O; while the b parameter remained around 0.20 - 0.26 $m^3 \cdot N^{-1} \cdot s^{-2}$ for the operating range evaluated (see Fig. 5c). According to this result, since viscosity correction was not necessary for laminar conditions, the a and b parameter values can be calculated as follows:

$$a = \begin{cases} (2.3260 \cdot 10^{-4} \cdot \mu - 5.6046 \cdot 10^{-2})_{Re>2100} \\ 0 \ _{Re<2100} \end{cases} \quad eq.(18)$$

$$b = \begin{cases} 0.23 \ _{Re>2100} \\ 0 \ _{Re<2100} \end{cases} \quad eq.(19)$$

According to the proposed model, although R_M cannot be considered negligible, R_T is mainly controlled by R_L (see Fig. 6), resulting in about 80-90% of the R_T. In this regard, Wickramasinghe *et al*. (1992) suggested that for oxygen-water separation by micro-porous membranes, the achieved k_M is significantly higher than k_L. Therefore, k_L dominates mass transfer in DMs, concluding that K_O is independent of membrane properties. Henares *et al.* (2017) also reported similar results when operating PDMS membranes for methane recovery, and concluded that the R_L contributes about 80% of R_T.

These authors also indicate that k_M can be positively influenced by the applied vacuum pressure in the permeate. Since the DM unit was operated at high permeate vacuum pressures (TMP = 0.8 bar) k_M could have been significantly improved, thus reducing the influence of R_M on R_T. Nonetheless, since many factors can affect K_O (e.g. temperature, Q_L:A, flow properties, TMP) further research is required to determine the influence of each partial resistance on R_T and develop strategies to improve mass transfer in DMs.

3.4. Energy balance and environmental impact of the DM unit and AnMBR+DM system

The energy recovery and GHG emissions of the DM unit were calculated in order to evaluate the feasibility of this technology for capturing the dissolved methane from anaerobic effluents, thus enhancing AnMBR performance for UWW treatment. Figs. 7a and 7b show the energy recovery and GHG emissions reached by the PDMS DM module under the operating conditions evaluated. As expected, net energy productions were achieved by the DM unit, which is in accordance with the results reported by other authors when using this technology for capturing the dissolved methane from anaerobic effluents (Cookney *et al.*, 2016; Henares *et al.*, 2017). The maximum energy recovery was achieved at the lowest temperature and the lowest Q_L:A. Temperature affected energy recovery due to its influence on methane flux (see Fig. 1a and 1b), so that for each Q_L:A the higher the permeated methane flux the higher the energy output. Moreover energy recovery improved as Q_L:A decreased due the higher MRE achieved (see Fig. 1c). Similarly, the lowest GHG emission was reached at the lowest Q_L:A and the highest temperature due to enhanced MRE under these conditions. However, since raising temperature reduced the influent dissolved methane, the beneficial effects of reducing Q_L:A on energy output and GHG emission mitigations are significatively reduced as

498 temperature increases. Maximum energy recoveries of about 0.13 kWh per m^3 of treated
499 water were achieved, which were similar to that reported by other authors. Specifically,
500 when operating PDMS DM units, Cookney *et al*. (2012; 2016) and Henares *et al*. (2017)
501 reported maximum energy recoveries of around 0.12 – 0.14 kWh per m^3 of treated water.
502 Therefore, the results obtained in this study confirms that these promising results can also
503 be achieved in higher-scale plants.

504 Finally, the total energy recovery and GHG emissions of the combined system
505 (AnMBR+DM) were calculated (energy demands and GHG emissions of the AnMBR
506 prototype plant operated at the temperature ranging studied can be found in the Appendix
507 A, Fig. A1). As show in Figs. 7c and 7d, energy savings can be significantly improved by
508 coupling a DM unit for dissolved methane capture especially at low temperatures and
509 GHG emissions are drastically reduced by the recovery of high-GWP gas. The
510 AnMBR+DM system gave maximum energy recovery and minimum GHG emissions of
511 about 0.18 kWh and 0.070 kg of CO_2-eq per m^3 of treated water, respectively in winter
512 (T = 11 ºC) and maximum energy recovery of about 0.87 kWh and net GHG emission
513 reductions of up to 0.216 kg CO_2–eq per m^3 of treated water in summer (T = 30 ºC). Since
514 the average energy demand of conventional activated sludge (CAS) processes is about
515 0.36 kWh per m^3 of treated water (Hao *et al*., 2018), the AnMBR+DM system could be
516 considered as a promising alternative for UWW treatment, being able to recover a
517 significant amount of energy from UWW through the conversion of biodegradable
518 organic carbon into methane. On the other hand, considering an average GHG indirect
519 emissions factor of around 0.3–0.4 kg CO_2–eq per kWh of input energy (Emami *et al*.,
520 2018), indirect GHG emissions of 0.108 – 0.144 kg CO_2–eq per m^3 of treated water could
521 be expected from CAS process. Moreover, other indirect GHG and direct GHG emissions
522 (N_2O and CH_4 gas) could significantly increase GHG emissions of CAS process

(Parravicini et al., 2016). Therefore, the combination of AnMBR with DMs represents an interesting alternative to significantly reduce the GHG emissions of UWW treatment. Indeed, making allowance of the evolution of climatic change worldwide, all countries are developing new and more demanding GHG emissions policies to confront this crisis (Eskander & Fankhauser, 2020). Unfortunately, the objectives established in the Paris Agreement are not on track to be met (Rogelj et al., 2016), auguring that GHG emissions for 2030 will be significantly higher than the ones required for the 2-ºC stabilization path estimated by the united nations (UNEP, 2019). In addition, finding sources of high quality reclaimed water is also a prominent issue in worldwide policies (Jiménez-Benítez *et al*., 2020). Therefore, considering the high quality effluent that AnMBR technology is able to produce for possible water reclamation, and the high energy recovery and low GHG emissions associated to this process after coupling a DM unit for dissolved methane recovery, the combination of AnMBR with DM for UWW treatment may be considered as an attractive option by regulators and policy makers, being able to provide important environmental, economic and social benefits.

4. CONCLUSIONS

The effect of the operating temperature and the hydrodynamics on the performance of a PDMS DM for capturing the dissolved methane from AnMBR effluents was evaluated. Moreover, the energy demand and carbon footprint of the combined system (AnMBR+DM) was assessed. The main findings were as follows:

- The DM unit showed a high potential for capturing the dissolved methane from the AnMBR system. Dissolved methane recovery was maximized at low Q_L:A ratios by the raise of the DM's HRT, achieving maximum methane capture

efficiencies of about 79 and 85% when operating at 11 and 30 ºC, respectively. Temperature could therefore be considered as not a limiter parameter for methane capture from anaerobic effluents.

- The calculated resistance of the DM system to methane permeation showed that K_O was improved at higher temperatures. This effect was attributed to improved methane diffusivity in water and PDMS under these conditions. The hydrodynamic analysis showed that the transition from laminar to turbulent flow reduced K_O. Since short-term fouling propensity was negligible, this effect was attributed to an increase in membrane fibers deformation as Q_L:A was raised.

- A theoretical resistance-in-series model was proposed to predict K_O in the DM module used in this study. Adequate predictions were reached under laminar conditions while an empirical correction was suggested under turbulent conditions to achieve properly predictions. According to the model, k_L would control mass flux, representing up to 80-90% of total mass flux resistance.

- Using DMs for dissolved methane capture significatively increase energy savings and reduce GHG emissions from AnMBRs. The AnMBR+DM system gave net energy productions and GHG emissions of about 0.18 kWh and 0.070 kg of CO_2-eq per m^3 of treated water, respectively, when operating at 11 ºC. Net energy productions of about 0.86 kWh and net GHG reductions of up to 0.216 kg CO_2–eq per m^3 of treated were achieved when operating at 30 ºC.

Based on the results achieved in this study, the use of AnMBR technology assisted by PDMS DMs could be considered as a potential alternative for UWW treatment. Nonetheless, important aspects need to be refined before their full-scale implementation, requiring further research:

- Due to the negative effects observed on K_O when increasing Q_L:A, further studies focused on improving DM's hydrodynamics and increasing DM's HRT are suggested in order to improve the methane capture effectivity. Different module configurations, membrane materials or multi-layer membranes could represent interesting options to be evaluated.

- Since only some hydrodynamic characteristics of the DM module were considered to model K_O, future research considering other DM configurations should be performed to evaluate the viability of the proposed model or to develop advanced models.

- Due to the low Q_L:A ratios required to maximize the dissolved methane recovery, important economic investments could be expected for the DM unit, although they could be partially counterbalanced by the increased energy recovery and reduced GHG emissions. Therefore, further studies considering all the economic aspects of the proposed alternative as well as deeper environmental evaluations (i.e. life cycle cost and life cycle assessment studies) need to be performed to determine the actual suitability of the AnMBR+DM alternative for UWW treatment.

ACKNOWLEDGEMENTS

This research work was supported by *Generalitat Valenciana* via Fellowships CPI-16-155 and C12747, as well as the financial aid received from the *Ministerio de Economía y Competitividad* via Juan de la Cierva Contract FJCI-2014-21616. This research work was also made possible thanks to co-financing by the European Financial Instrument for the Environment (LIFE+) during the implementation of the Project Membrane for ENERGY and WATER RECOVERY "MEMORY" (LIFE13 ENV/ES/001353).

Nomenclature

A	Fitting parameter of Himmelblau's equation
a	Fitting parameter of the linear equation proposed in this study to correct the liquid phase mass transfer coefficient under turbulent conditions
A_M	Membrane area
A_G	Effective membrane area interacting with the gas phase
A_L	Effective membrane area interacting with the liquid phase
A_{ml}	Logarithmic mean area of the degassing membrane
AnMBR	Anaerobic membrane bioreactor
B	Fitting parameter of Himmelblau's equation
b	Fitting parameter of the linear equation proposed in this study to correct the liquid phase mass transfer coefficient under turbulent conditions
c	Concentration of the diffused compound
c_{CH4}	Dissolved methane concentration in the water
$c_{CH4.inf}$	Concentration of dissolved methane in the influent membrane stream
$c_{CH4.eff}$	Concentration of dissolved methane in the effluent membrane stream
c_G	Methane concentration in the gas phase
c^*_{CH4}	Membrane-gas interphase methane concentration
D	Diffusion coefficient
$D_{CH4-PDMS}$	Methane diffusivity in polydimethylsiloxane
D_{CH4-W}	Methane diffusivity in water
D_{eq}	Equivalent diameter
DM	Degassing membrane
E_P	Fitting parameter of Van't Hoff–Arrhenius's equation
GHG	Greenhouse gas
$H^{CH4}(T)$	Henrry's constant for methane
J	Flux of the diffused compound
J_{CH4}	Permeated methane flux
k_G	Mass transfer coefficient of the recovered gas in the gas phase
k_L	Mass transfer coefficient of the recovered gas in the liquid phase
k_M	Mass transfer coefficient of the recovered gas in the permeable membrane
K_O	Overall mass transfer coefficient of the system

L_w	Wet fiber length
MRE	methane recovery efficiency
P	Permeability
$P_{CH4\text{-}PDMS}$	Methane permeability in polydimethylsiloxane
PDMS	Polydimethylsiloxane
P_0	Fitting parameter of Van't Hoff–Arrhenius's equation
Q_L	Liquid flow rate
Q_L:A	Liquid flow rate to membrane area
R	Universal constant of gases
Re	Reynolds module
R_G	Gas boundary layer resistance
R_L	Liquid boundary layer resistance
R_M	Permeable non-porous membrane resistance
R_T	Total mass flux resistance
S	Solubility coefficient
Sc	Schmidt dimensionless module
$S_{CH4\text{-}PDMS}$	Methane solubility in polydimethylsiloxane
Sh	Sherwood dimensionless module
T	Temperature
TC	Total carbon
TIC	Total inorganic carbon
t_L	Thickness of the liquid phase resistance
t_M	Membrane thickness
TOC	Total organic carbon
UWW	Urban wastewater
V_{cd}	Cylindrical diffuser volume
V_S	Shell volume
v_L	Liquid velocity
x	Distance between two points
Greek Letters	
μ	Liquid viscosity

593

REFERENCES

Alexander Stern, S. Polymers for gas separations: the next decade, J. Memb. Sci. 94 (1994) 1–65. https://doi.org/10.1016/0376-7388(94)00141-3.

APHA, A., WEF, (2012). Standard Methods for the Examination of Waters and Wastewaters, 22st ed. American Public Health Association/American Water Works Association/Water Environmental Federation Washington DC, USA.

Bandara, W. M. K. R. T. W., Ikeda, M., Satoh, H., Sasakawa, M., Nakahara, Y., Takahashi, M., & Okabe, S. (2013). Introduction of a Degassing Membrane Technology into Anaerobic Wastewater Treatment. *Water Environment Research*, *85*(5), 387–390. https://doi.org/10.2175/106143013x13596524516707

Bandara, W. M. K. R. T. W., Kindaichi, T., Satoh, H., Sasakawa, M., Nakahara, Y., Takahashi, M., & Okabe, S. (2012). Anaerobic treatment of municipal wastewater at ambient temperature: Analysis of archaeal community structure and recovery of dissolved methane. Water Research, 46(17), 5756–5764. https://doi.org/10.1016/j.watres.2012.07.061

Bandara, Wasala M.K.R.T.W., Satoh, H., Sasakawa, M., Nakahara, Y., Takahashi, M., & Okabe, S. (2011). Removal of residual dissolved methane gas in an upflow anaerobic sludge blanket reactor treating low-strength wastewater at low temperature with degassing membrane. *Water Research*, *45*(11), 3533–3540. https://doi.org/10.1016/j.watres.2011.04.030

Bani Shahabadi, M., Yerushalmi, L., & Haghighat, F. (2009). Impact of process design on greenhouse gas (GHG) generation by wastewater treatment plants. *Water Research*, *43*(10), 2679–2687. https://doi.org/10.1016/j.watres.2009.02.040

Chen, Y. A., Chu, C. K., Chen, Y. P., Chu, L. S., Lin, S. T., & Chen, L. J. (2018). Measurements of diffusion coefficient of methane in water/brine under high

pressure. *Terrestrial, Atmospheric and Oceanic Sciences*, *29*(5), 577–587. https://doi.org/10.3319/TAO.2018.02.23.02

Cookney, J. (2011). Methane management in sewage treatment. *Ph.D. thesis. School of applied sciences. Cranfield university, United kingdom.*

Cookney, J., Cartmell, E., Jefferson, B., & McAdam, E. J. (2012). Recovery of methane from anaerobic process effluent using poly-di-methyl-siloxane membrane contactors. *Water Science and Technology*, *65*(4), 604–610. https://doi.org/10.2166/wst.2012.897

Cookney, J., Mcleod, A., Mathioudakis, V., Ncube, P., Soares, A., Jefferson, B., & McAdam, E. J. (2016). Dissolved methane recovery from anaerobic effluents using hollow fibre membrane contactors. *Journal of Membrane Science*, 502, 141–150.

Crone, B. C., Garland, J. L., Sorial, G. A., & Vane, L. M. (2017). Corrigendum to "Significance of dissolved methane in effluents of anaerobically treated low strength wastewater and potential for recovery as an energy product: A review" [Water Res. 104 (2016) 520–531](S0043135416306194)(10.1016/j.watres.2016.08.019). *Water Research*, *111*, 420. https://doi.org/10.1016/j.watres.2017.01.035

Emami, N., Sobhani, R., & Rosso, D. (2018). Diurnal variations of the energy intensity and associated greenhouse gas emissions for activated sludge processes. Water Science and Technology, 77(7), 1838–1850. https://doi.org/10.2166/wst.2018.054

Eskander, S. M. S. U., & Fankhauser, S. (2020). Reduction in greenhouse gas emissions from national climate legislation. Nature Climate Change, 10(8), 750–756. https://doi.org/10.1038/s41558-020-0831-z

Favre, E. (2017). Polymeric Membranes for Gas Separation. Elsevier B.V. Nancy Université, France.

Giménez, J. B., Martí, N., Ferrer, J., & Seco, A. (2012). Methane recovery efficiency in

644 a submerged anaerobic membrane bioreactor (SAnMBR) treating sulphate-rich
645 urban wastewater: Evaluation of methane losses with the effluent. *Bioresource*
646 *Technology*, *118*, 67–72. https://doi.org/10.1016/j.biortech.2012.05.019

647 Giménez, J. B., Martí, N., Robles, A., Ferrer, J., & Seco, A. (2014). Anaerobic treatment
648 of urban wastewater in membrane bioreactors: Evaluation of seasonal temperature
649 variations. *Water Science and Technology*, 69(7), 1581–1588.
650 https://doi.org/10.2166/wst.2014.069

651 Hao, X. D., Li, J., Van Loosdrecht, M. C. M., & Li, T. Y. (2018). A sustainability-based
652 evaluation of membrane bioreactors over conventional activated sludge processes.
653 Journal of Environmental Chemical Engineering, 6(2), 2597–2605.
654 https://doi.org/10.1016/j.jece.2018.03.050

655 Henares, M., Izquierdo, M., Marzal, P., & Martínez-Soria, V. (2017). Demethanization
656 of aqueous anaerobic effluents using a polydimethylsiloxane membrane module:
657 Mass transfer, fouling and energy analysis. *Separation and Purification Technology*,
658 186, 10–19.

659 Henares, M., Izquierdo, M., Penya-Roja, J. M., & Martínez-Soria, V. (2016).
660 Comparative study of degassing membrane modules for the removal of methane
661 from Expanded Granular Sludge Bed anaerobic reactor effluent. *Separation and*
662 *Purification Technology*, 170, 22–29.

663 Himmelblau, D. M., 1964: Diffusion of dissolved gases in liquids. Chem. Rev., 64, 527-
664 550, doi: 10.1021/cr60231a002

665 Jiménez-Benítez, A., Ferrer, F. J., Greses, S., Ruiz-Martínez, A., Fatone, F., Eusebi, A.
666 L., … Seco, A. (2020). AnMBR, reclaimed water and fertigation: Two case studies
667 in Italy and Spain to assess economic and technological feasibility and CO2
668 emissions within the EU Innovation Deal initiative. Journal of Cleaner Production,

669 270. https://doi.org/10.1016/j.jclepro.2020.122398
670 Jiménez-Benítez, A., Ferrer, J., Rogalla, F., Vázquez, J.R., Seco, A., Robles, Á. (2020)
671 Energy and environmental impact of an anaerobic membrane bioreactor (AnMBR)
672 demonstration plant treating urban wastewater, Curr. Dev. Biotechnol. Bioeng.
673 (2020) 289–310. https://doi.org/10.1016/b978-0-12-819854-4.00012-5.
674 Lee, M., Keller, A. A., Chiang, P. C., Den, W., Wang, H., Hou, C. H., … Yan, J. (2017).
675 Water-energy nexus for urban water systems: A comparative review on energy
676 intensity and environmental impacts in relation to global water risks. *Applied*
677 *Energy*, *205*, 589–601. https://doi.org/10.1016/j.apenergy.2017.08.002
678 Lettinga, G., Rebac, S., Zeeman, G., 2001. Challenge of psychrophilic anaerobic
679 wastewater treatment. Trends Biotechnol. 19, 363–370.
680 Lu, J. G., Zheng, Y. F., Cheng, M. D. (2008). Wetting mechanism in mass transfer process
681 of hydrophobic membrane gas absorption. *Journal of Membrane Science* 308, 180-
682 190.
683 McCarty, P. L., Bae, J., & Kim, J. (2011). Domestic wastewater treatment as a net energy
684 producer - can this be achieved? *Environmental Science & Technology*, *45*(17),
685 7100–7106. https://doi.org/10.1021/es2014264
686 Olhoff, A., & Christensen, J. M. (Eds.) (2019). Emissions Gap Report 2019. United
687 Nations Environment Programme (UNEP).
688 Parravicini, V., Svardal, K., & Krampe, J. (2016). Greenhouse Gas Emissions from
689 Wastewater Treatment Plants. Energy Procedia, 97, 246–253.
690 https://doi.org/10.1016/j.egypro.2016.10.067
691 Pinnau, I., & He, Z. (2004). Pure- and mixed-gas permeation properties of
692 polydimethylsiloxane for hydrocarbon/methane and hydrocarbon/hydrogen

693 separation. *Journal of Membrane Science*, 244(1–2), 227–233.
694 Pretel, R., Durán, F., Robles, A., Ruano, M. V., Ribes, J., Serralta, J., & Ferrer, J. (2015).
695 Designing an AnMBR-based WWTP for energy recovery from urban wastewater:
696 The role of primary settling and anaerobic digestion. *Separation and Purification*
697 *Technology*, *156*, 132–139. https://doi.org/10.1016/j.seppur.2015.09.047
698 Pretel, R., Robles, A., Ruano, M. V., Seco, A., & Ferrer, J. (2016). A plant-wide energy
699 model for wastewater treatment plants: application to anaerobic membrane
700 bioreactor technology. *Environmental Technology (United Kingdom)*, *37*(18), 2298–
701 2315. https://doi.org/10.1080/09593330.2016.1148903
702 Raharjo, R. D., Freeman, B. D., Paul, D. R., Sarti, G. C., & Sanders, E. S. (2007a). Pure
703 and mixed gas CH4 and n-C4H10 permeability and diffusivity in
704 poly(dimethylsiloxane). *Journal of Membrane Science*, *306*(1–2), 75–92.
705 https://doi.org/10.1016/j.memsci.2007.08.014
706 Raharjo, R. D., Freeman, B. D., & Sanders, E. S. (2007b). Pure and mixed gas CH4 and
707 n-C4H10 sorption and dilation in poly(dimethylsiloxane). *Journal of Membrane*
708 *Science*, *292*(1–2), 45–61. https://doi.org/10.1016/j.memsci.2007.01.012
709 Robles, Á., Ruano, M. V., Charfi, A., Lesage, G., Heran, M., Harmand, J., … Ferrer, J.
710 (2018). A review on anaerobic membrane bioreactors (AnMBRs) focused on
711 modelling and control aspects. *Bioresource Technology*, *270*(September), 612–626.
712 https://doi.org/10.1016/j.biortech.2018.09.049
713 Rogelj, J. et al. (2016). Paris Agreement climate proposals need a boost to keep warming
714 well below 2 °C. Nature 534, 7609–7631.
715 Sadrzadeh, M., Shahidi, K., & Mohammadi, T. (2009). Effect of operating parameters on
716 pure and mixed gas permeation properties of a synthesized composite PDMS/PA
717 membrane. *Journal of Membrane Science*, *342*(1–2), 327–340.

https://doi.org/10.1016/j.memsci.2009.07.015

Sanchis-Perucho, P., Robles, Á., Durán, F., Ferrer, J., & Seco, A. (2020). PDMS membranes for feasible recovery of dissolved methane from AnMBR effluents. *Journal of Membrane Science*, *604* (March). https://doi.org/10.1016/j.memsci. 2020.118070

Smith, A. L., Stadler, L. B., Love, N. G., Skerlos, S. J., & Raskin, L. (2012). Perspectives on anaerobic membrane bioreactor treatment of domestic wastewater: A critical review. *Bioresource Technology*, *122*, 149–159. https://doi.org/10.1016/j.biortech.2012.04.055

Stanojević, M., Lazarević, B., Radić, D. (2003). Review of membrane contactors designs and applications of different modules in industry. *FME Trans.* 31, 91–98.

Stazi, V., Tomei, M.C. (2018) Enhancing anaerobic treatment of domestic wastewater: State of the art, innovative technologies and future perspectives, Sci. Total Environ. 635 78–91. https://doi.org/10.1016/j.scitotenv.2018.04.071.

Tremblay, P., Savard, M. M., Vermette, J., & Paquin, R. (2006). Gas permeability, diffusivity and solubility of nitrogen, helium, methane, carbon dioxide and formaldehyde in dense polymeric membranes using a new on-line permeation apparatus. *Journal of Membrane Science*, *282*(1–2), 245–256. https://doi.org/10.1016/j.memsci.2006.05.030

Velasco, P., Jegatheesan, V., & Othman, M. (2018). Recovery of dissolved methane from anaerobic membrane bioreactor using degassing membrane contactors. *Frontiers in Environmental Science*, *6*(DEC), 1–6. https://doi.org/10.3389/fenvs.2018.00151

Wickramasinghe, S. R., Semmens, M. J., & Cussler, E. L. (1992). Mass transfer in various hollow fiber geometries. *Journal of Membrane Science*, *69*(3), 235–250. https://doi.org/10.1016/0376-7388(92)80042-I

Wickramasinghe, S. R., Semmens, M. J., & Cussler, E. L. (1993). Hollow fiber modules made with hollow fiber fabric. *Journal of Membrane Science*, *84*(1–2), 1–14. https://doi.org/10.1016/0376-7388(93)85046-Y

Table and Figure captions

Table 1. DM influent and effluent characteristics according to applied Q_L:A ratio (11 ºC operating temperature).

Fig. 1. Methane recovery for the operating conditions studied: (a) Recovered methane flux for a Q_L:A ranging from 22 to 118 $Lh^{-1}m^{-2}$, (b) Recovered methane flux for a Q_L:A ranging from 142 to 190 $Lh^{-1}m^{-2}$ and (c) Methane recovery efficiency. ▫ Q_L:A of 22 $Lh^{-1}m^{-2}$; ◆ Q_L:A of 46 $Lh^{-1}m^{-2}$; ▲ Q_L:A of 70 $Lh^{-1}m^{-2}$; × Q_L:A of 94 $Lh^{-1}m^{-2}$; – Q_L:A of 118 $Lh^{-1}m^{-2}$; ○ Q_L:A of 142 $Lh^{-1}m^{-2}$; + Q_L:A of 166 $Lh^{-1}m^{-2}$; ✖ Q_L:A of 190 $Lh^{-1}m^{-2}$.

Fig. 2. Influence of temperature and hydrodynamics on the overall mass transfer coefficient (K_O). Influence of: (a) Q_L and v_L, and (b) Reynolds number.

Fig. 3. Effect of DM operating time and Q_L:A ratio on membrane fouling (11 ºC operating temperature).

Fig. 4. Model validation at Q_L:A of: (a) 22, (b) 46, (c) 70, (d) 94, (e) 118, (f) 142, (g) 166 and (h) 190 L h^{-1} m^{-2}. Experimental results shown by dots and model predictions by continuous lines.

Fig. 5. Fitting parameters of the model as a function of Q_L:A ratio: (a) A and B parameters (*eq.* 10), (b) P_0, E_P and t_L parameters (*eq.* 10) and (c) a and b parameters (*eq.* 17). Dotted lines show a linear fit.

Fig. 6. Evolution of the liquid, membrane and overall mass transfer coefficient calculated from the proposed theoretical model according to temperature and Q_L:A ratio.

Fig. 7. Influence of temperature and Q_L:A ratio on: (a) DM energy demand, (b) DM GHG emissions, (c) DM+AnMBR system energy demand and (d) DM+AnMBR system GHG emissions. ▫ Q_L:A of 22 $Lh^{-1}m^{-2}$; ◆ Q_L:A of 46 $Lh^{-1}m^{-2}$; ▲ Q_L:A of 70 $Lh^{-1}m^{-2}$; × Q_L:A of 94 $Lh^{-1}m^{-2}$; – Q_L:A of 118 $Lh^{-1}m^{-2}$; ○ Q_L:A of 142 $Lh^{-1}m^{-2}$; + Q_L:A of 166 $Lh^{-1}m^{-2}$; ✖ Q_L:A of 190 $Lh^{-1}m^{-2}$.

Table 1. DM influent and effluent characteristics according to applied Q_L:A ratio (11 ºC operating temperature).

Stream	Q_L:A ($Lh^{-1}m^{-2}$)	pH	NH_4^--N ($mgN\ L^{-1}$)	PO_4^{3-}-P ($mgP\ L^{-1}$)	TIC ($mgC\ L^{-1}$)	TOC* ($mgC\ L^{-1}$)
Influent	-	7.1 ± 0.3	54.5 ± 0.4	5.0 ± 0.3	273.7 ± 54	64.4 ± 9
Effluent	25	7.5± 0.2	55.8 ± 1.8	5.5 ± 0.1	268.1 ± 43	54.5 ± 12
	50	7.8± 0.3	54.3 ± 0.1	5.2 ± 0.2	n.a.	n.a.
	95	7.7± 0.2	51.9 ± 0.3	4.6 ± 0.3	268.8 ± 61	59.2 ± 15
	140	7.7± 0.2	52.0 ± 0.4	5.6 ± 0.7	n.a.	n.a.
	190	7.6± 0.3	51.4 ± 1.1	4.8 ± 0.5	268.7 ± 22	57.4 ± 8

*TOC concentration excluding dissolved methane.

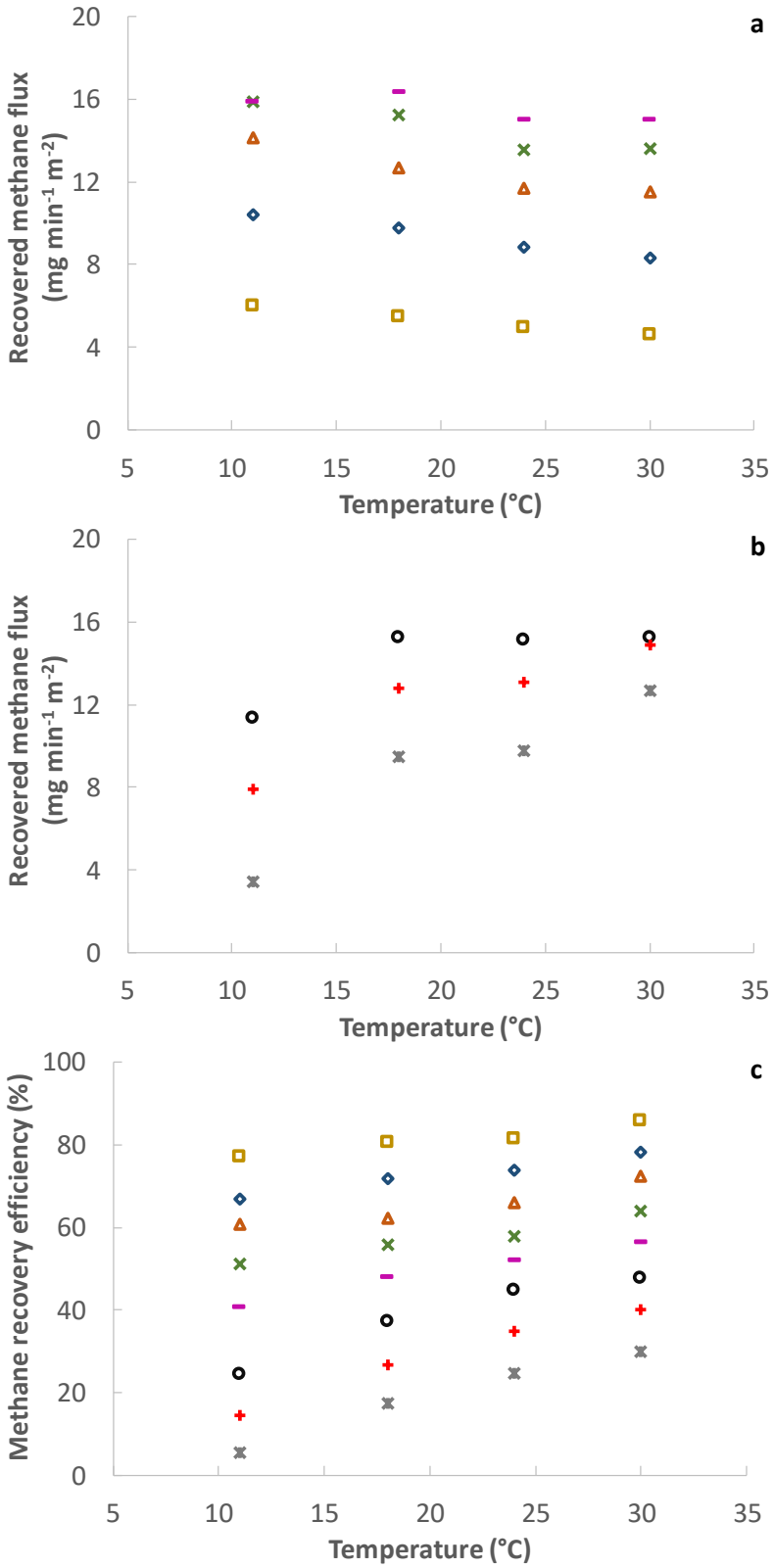

Fig. 1. Methane recovery for the operating conditions studied: (a) Recovered methane flux for a Q_L:A ranging from 22 to 118 $Lh^{-1}m^{-2}$, (b) Recovered methane flux for a Q_L:A ranging from 142 to 190 $Lh^{-1}m^{-2}$ and (c) Methane recovery efficiency. Q_L:A of 22 $Lh^{-1}m^{-2}$; Q_L:A of 46 $Lh^{-1}m^{-2}$; Q_L:A of 70 $Lh^{-1}m^{-2}$; Q_L:A of 94 $Lh^{-1}m^{-2}$; Q_L:A of 118 $Lh^{-1}m^{-2}$; Q_L:A of 142 $Lh^{-1}m^{-2}$; Q_L:A of 166 $Lh^{-1}m^{-2}$; Q_L:A of 190 $Lh^{-1}m^{-2}$.

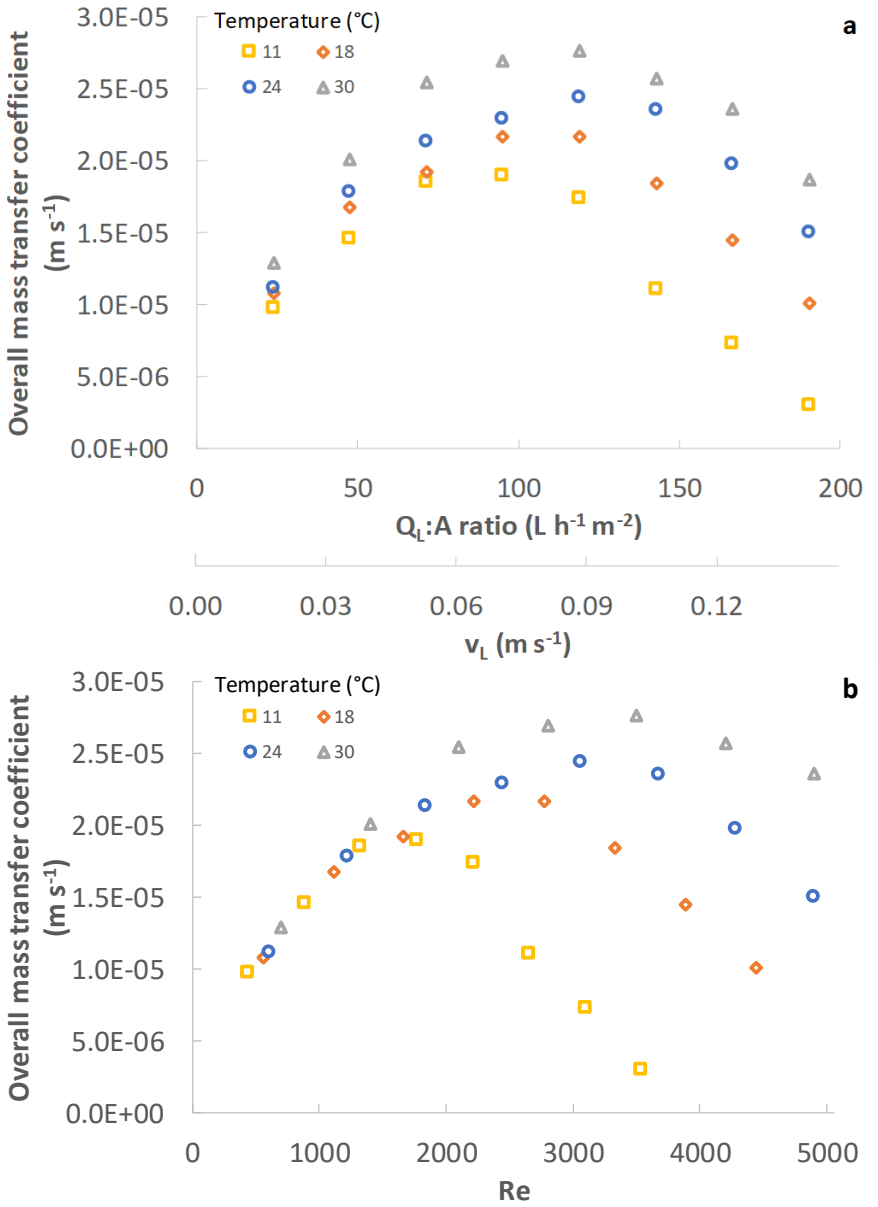

Fig. 2. Influence of temperature and hydrodynamics on the overall mass transfer coefficient (K_O). Influence of: (a) Q_L and v_L, and (b) Reynolds number.

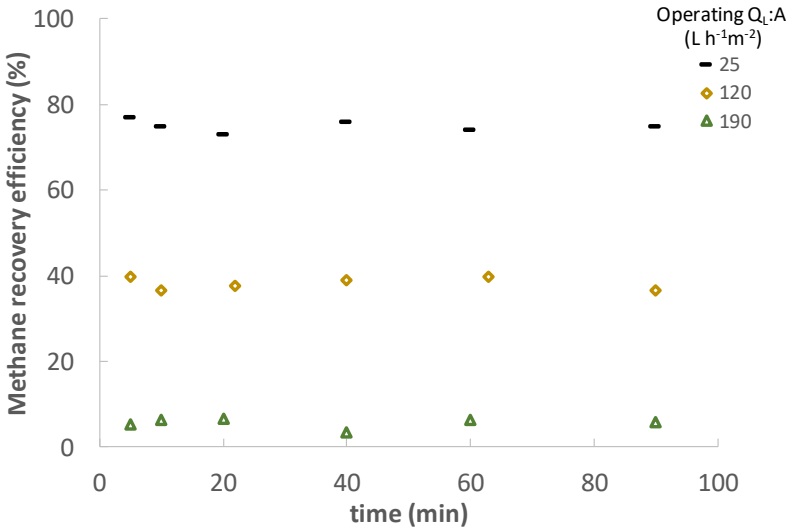

Fig. 3. Effect of DM operating time and Q_L:A ratio on membrane fouling (11 ºC operating temperature).

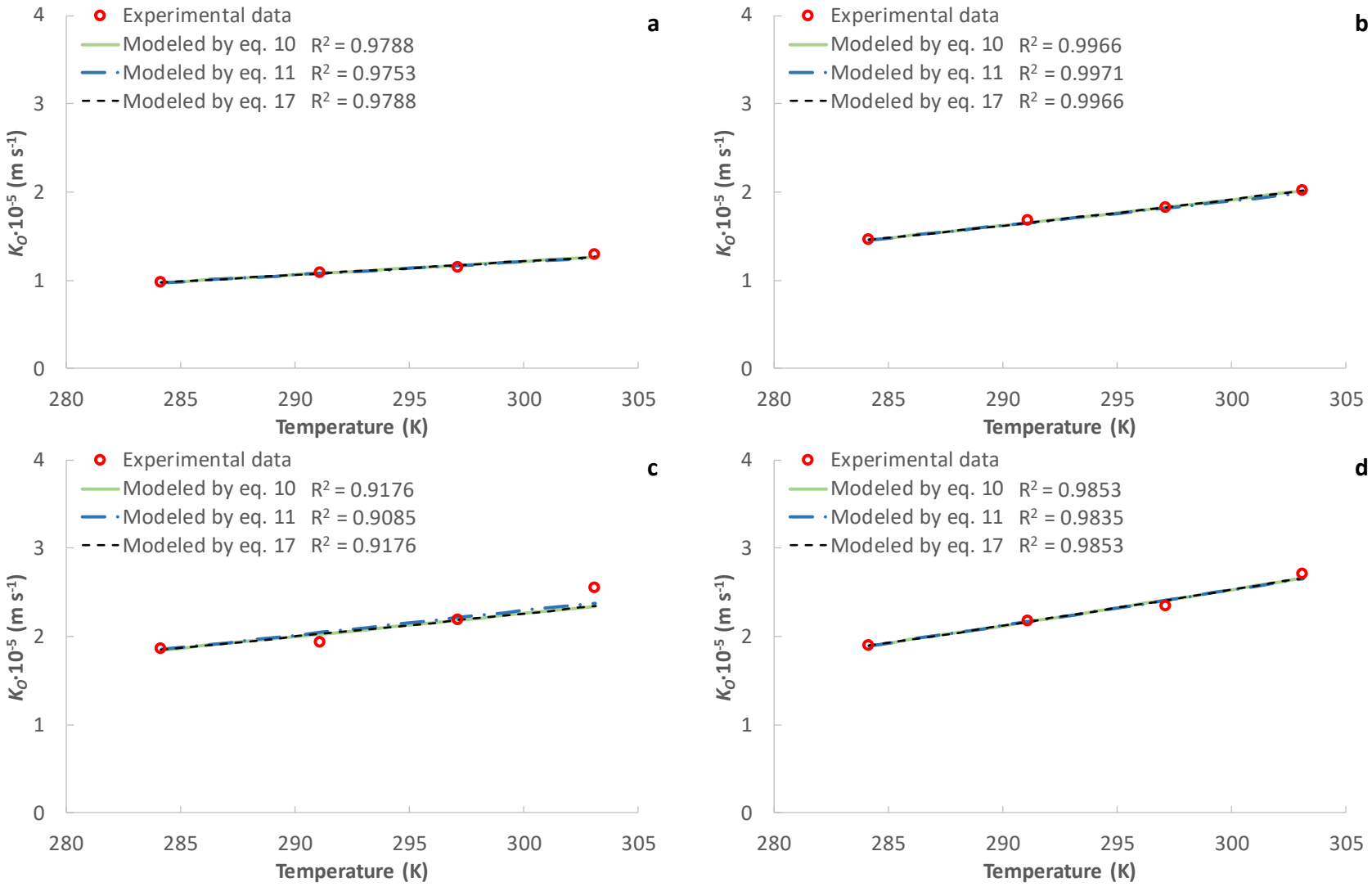
a
Experimental data
Modeled by eq. 10 R² = 0.9788
Modeled by eq. 11 R² = 0.9753
Modeled by eq. 17 R² = 0.9788
b
Experimental data
Modeled by eq. 10 R² = 0.9966
Modeled by eq. 11 R² = 0.9971
Modeled by eq. 17 R² = 0.9966
c
Experimental data
Modeled by eq. 10 R² = 0.9176
Modeled by eq. 11 R² = 0.9085
Modeled by eq. 17 R² = 0.9176
d
Experimental data
Modeled by eq. 10 R² = 0.9853
Modeled by eq. 11 R² = 0.9835
Modeled by eq. 17 R² = 0.9853
$K_O \cdot 10^{-5}$ (m s^{-1})
Temperature (K)
0
1
2
3
4
280
285
290
295
300
305

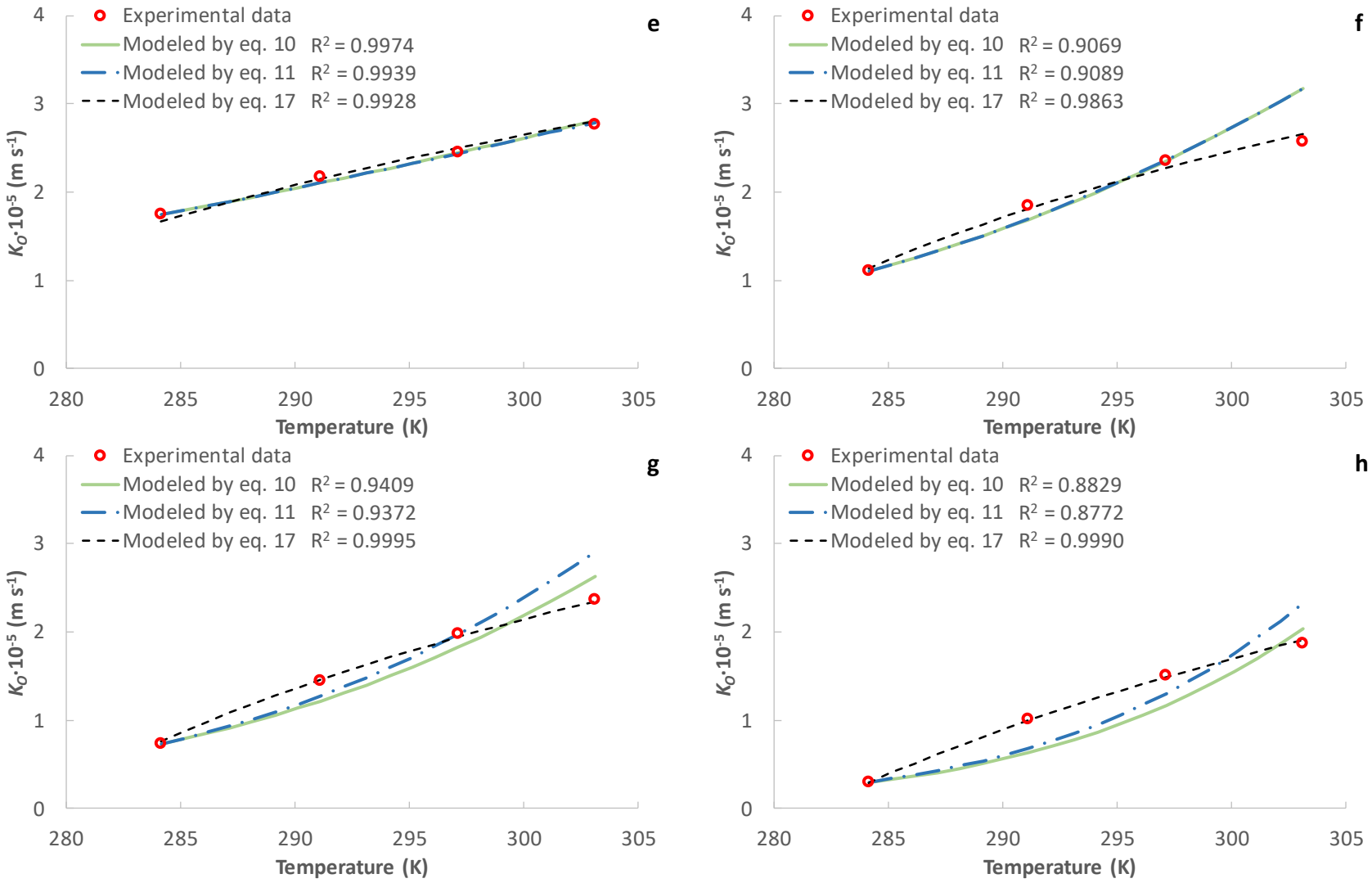

Fig. 4. Model validation at Q_L:A of: (a) 22, (b) 46, (c) 70, (d) 94, (e) 118, (f) 142, (g) 166 and (h) 190 L h^{-1} m^{-2}. Experimental results shown by dots and model predictions by continuous lines.

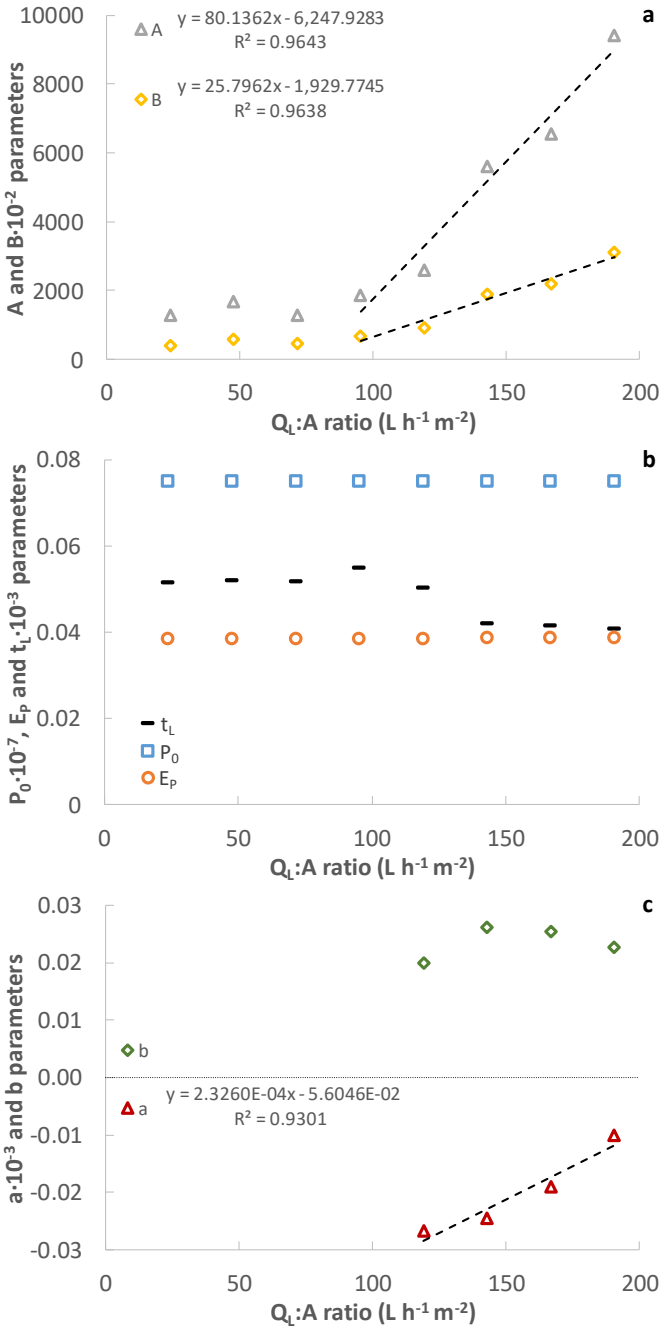

838

839

840

841 **Fig. 5.** Fitting parameters of the model as a function of Q_L:A ratio: (a) A and B parameters (*eq.* 10), (b)

842 P_0, E_P and t_L parameters (*eq.* 10) and (c) a and b parameters (*eq.* 17). Dotted lines show a linear fit.

843

844

845

846

847

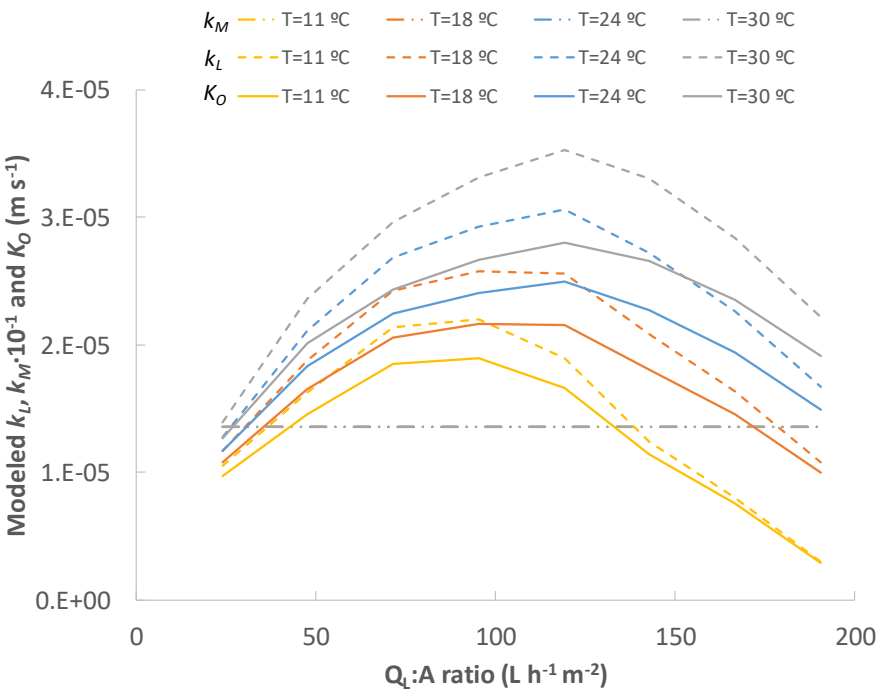

Fig. 6. Evolution of the liquid, membrane and overall mass transfer coefficient calculated from the proposed theoretical model according to temperature and Q_L:A ratio.

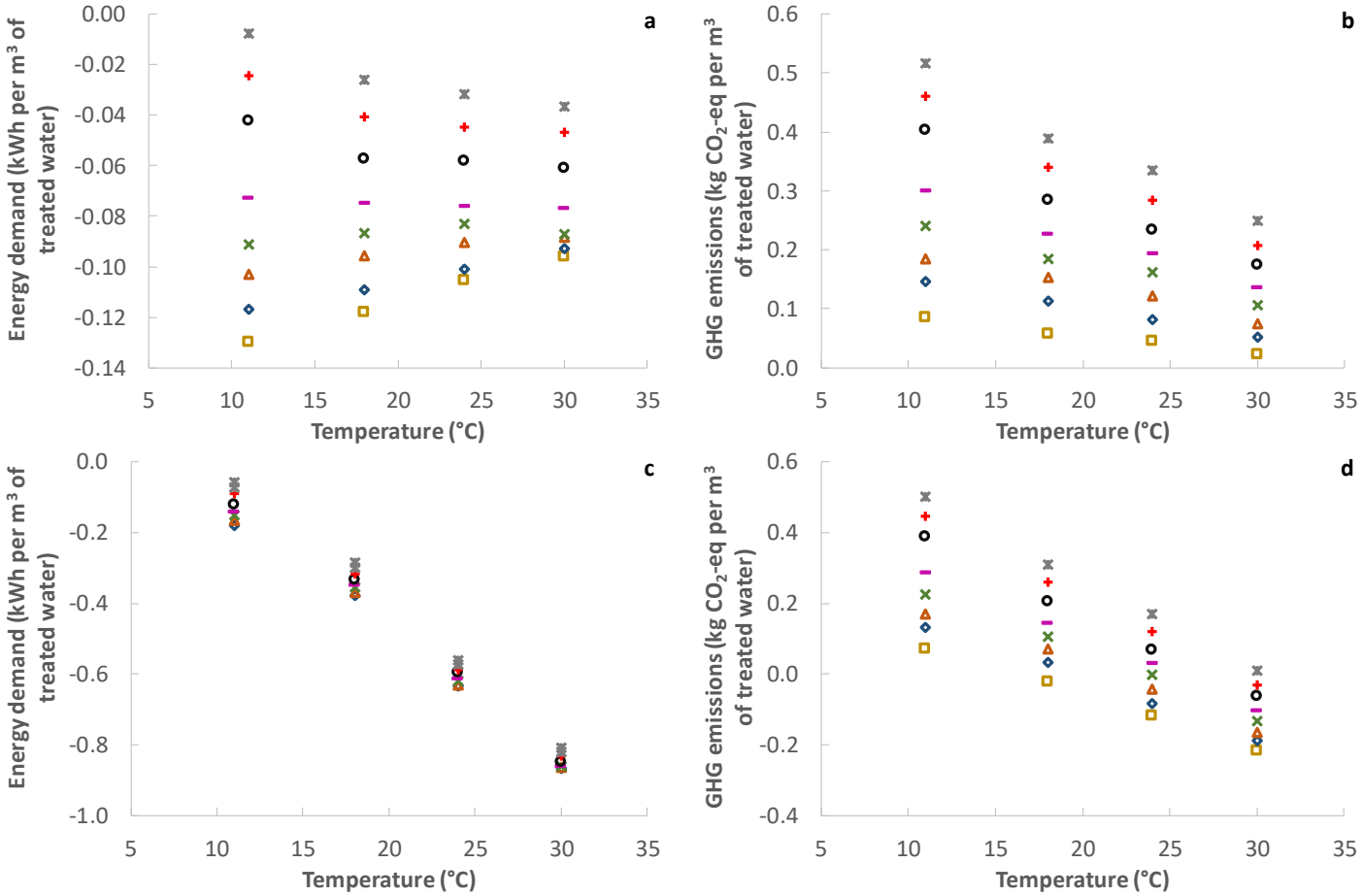

866 **Fig. 7.** Influence of temperature and Q_L:A ratio on: (a) DM energy demand, (b) DM GHG emissions, (c)
867 DM+AnMBR system energy demand and (d) DM+AnMBR system GHG emissions. ▫ Q_L:A of 22 $Lh^{-1}m^{-2}$; ◆ Q_L:A of 46 $Lh^{-1}m^{-2}$; ▲ Q_L:A of 70 $Lh^{-1}m^{-2}$; × Q_L:A of 94 $Lh^{-1}m^{-2}$; – Q_L:A of 118 $Lh^{-1}m^{-2}$; ○
869 Q_L:A of 142 $Lh^{-1}m^{-2}$; + Q_L:A of 166 $Lh^{-1}m^{-2}$; ✖ Q_L:A of 190 $Lh^{-1}m^{-2}$.